Electronic Supporting Information

Understanding aqueous organic redox flow batteries: a guided experimental tour from components characterization to final assembly.

J. Asenjo-Pascual,[a,*] I. Salmeron-Sanchez,[a] J. R. Aviles Moreno,[a] P. Mauleón,[b] P. Mazur [c, d] and P. Ocón.[a]

[a] Departamento de Química Física Aplicada, Universidad Autónoma de Madrid (UAM), C/Francisco Tomás y Valiente 7, 28049 Madrid, Spain;

[b] Departamento de Química Orgánica, Universidad Autónoma de Madrid (UAM), C/Francisco Tomás y Valiente 7, 28049 Madrid, Spain

[c] Faculty of Chemical Engineering, University of Chemistry and Technology, 166 28 Prague 6, Prague, Czech Republic

[d] New Technologies—Research Centre, University of West Bohemia, Univerzitní 8, 306 14 Plzeň, Czech Republic

* Correspondence: juan.asenjo@uam.es

Content list:

1. Experimental

1.1 Instruments and reagents

Unless otherwise noted, reagents and materials were purchased from commercial suppliers and used without further purification. Glassy carbon (3 mm) was used as working electrode for all three-electrode cell measurements (CV). Glassy carbon RDE (3 mm) was controlled by a Metrohm Autolab Motor Controller in LSV measurements. Pt

wire and Ag/AgCl (3M KCl) were used as counter and reference electrodes, respectively. Both CV and RDE tests were performed using an Autolab electrochemical system II PGSTAT30 potentiostat. The setting used on each technique is included in the caption of each figure. The solubilities were measured using an UV–Vis spectrophotometer (PerkinElmer, Lambda 365). The RFB single-cell was characterized at room temperature using a Biologic multichannel potentiostatic-galvanostatic coupled to an impedance module BSC-815.

1.2 Pourbaix diagram

Cyclic voltammetries were measured of a 10 mM of AQDS in 0.04 M universal or Briton-Robinson buffer (0.04 M of H_3PO_4, H_3BO_3 and acetic acid) at different pH (by adjusting the pH values with 0.1 M of HCl and 0.1 M of NaCl) set-up described in section 1.1 at 50mV/s potential scan rate and room temperature.

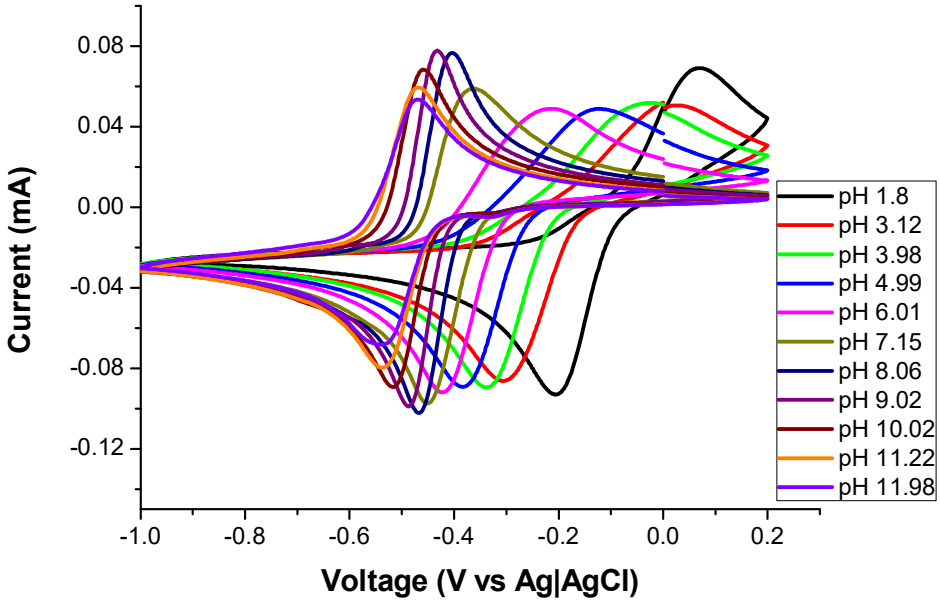

Figure S1: CV of 10 mM AQDS solution measured on glassy carbon working electrode (WE) at 100 mV/s, using Pt wire as counter electrode and Ag/AgCl as reference electrode at different pH values.

1.3 Kinetics parameters evaluation

Rotating Disk Electrode (RDE) measurements and Kinetic analysis

The diffusion coefficient was calculated from LSV measurements of 10mM AQDS 1M NaCl solution on RDE set-up described in section 1.1 using the Levich approximation as given in Eq. S1.

$$I_L = 0.620nFAD^{2/3}v^{-1/6}\omega^{1/2} \quad \text{(S1)}$$

Where I_L is the limiting current (A), n is the number of electrons involved in the redox reaction, F is the Faraday constant (C/mol), A is the electrode area (cm^2), D is the diffusion coefficient (cm^2/s), υ is the kinematic viscosity (cm^2/s) and ω the angular rotation rate of the electrode (rad/s).

Koutecký-Levich analysis of the same LSV data was performed according to Eq. S2

$$\frac{1}{i} = \frac{1}{i_k} + \frac{1}{0.620nFAD^{2/3}v^{-1/6}\omega^{1/2}C_o} \quad \text{(S2)}$$

$$\ln i_K = \ln nFC_oAk_o + \frac{\alpha nF\eta}{RT} \quad \text{(S3)}$$

$$\ln k_f = \ln k_o + \frac{\alpha nF\eta}{RT} \quad \text{(S4)}$$

Where I_K is the kinetic current (A), C_o is the molar concentration of the redox active material (mol/cm^3), α is the transfer coefficient, k_o is the kinetic constant (cm/s), η is the overpotential (V), R is the gas constant (J/mol·K) and T the temperature (K).

The I_K at low overpotentials were obtained by extrapolation of current values to infinite rotation rate and they were fitted to the Butler-Volmer equation (see Eq. S3) to get the standard rate constant of the reduction process, k_o.

Note that **3** and **6** materials have not been measured because of the irreversible character of the redox process. Compound **8** present low solubility, so it has been also excluded as potential electrolyte.

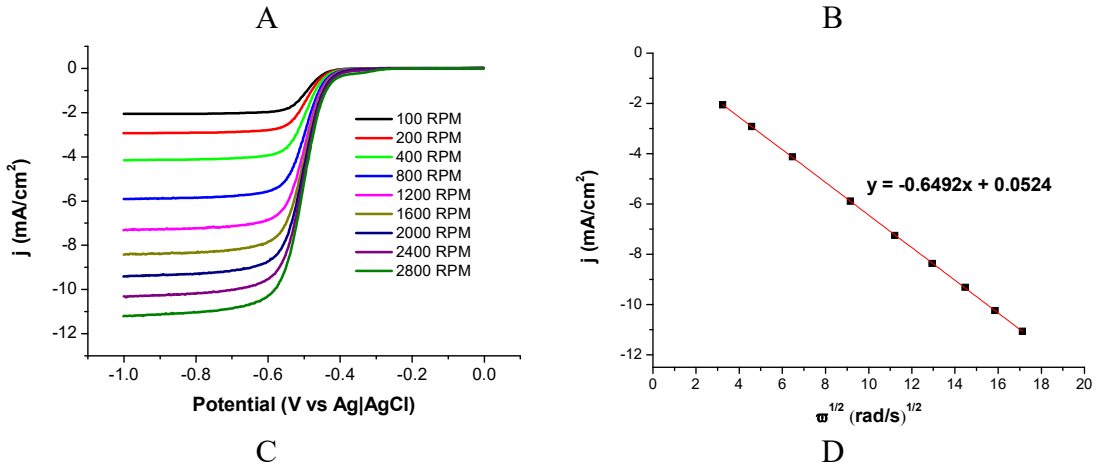

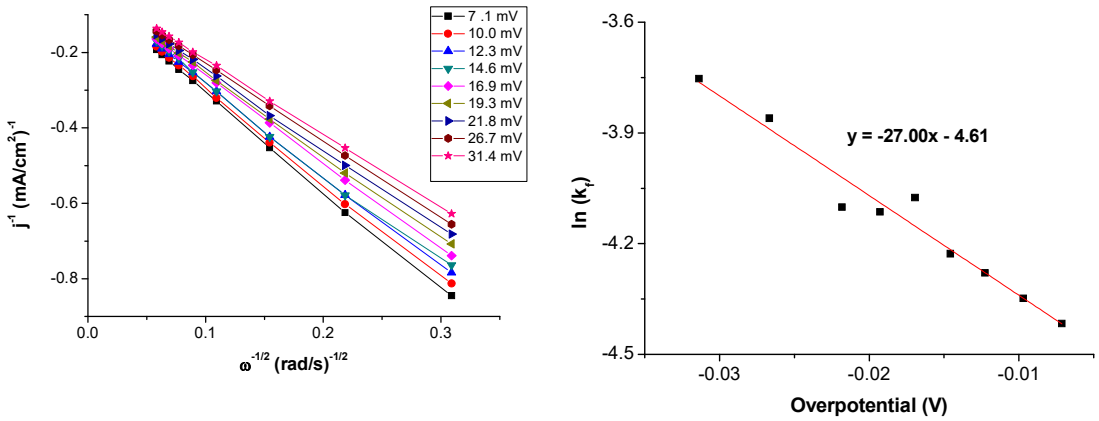

Figure S2: RDE analysis of **AQDS** 10mM in 1M NaCl electrolyte on glassy carbon working electrode: (a) LSV scans with rotating disc working electrode; Scan rate: 5 mV/s (b) Levich analysis of the reduction limiting currents; (c) Koutecký-Levich plot (b) and Tafel-plot for different overpotentials.

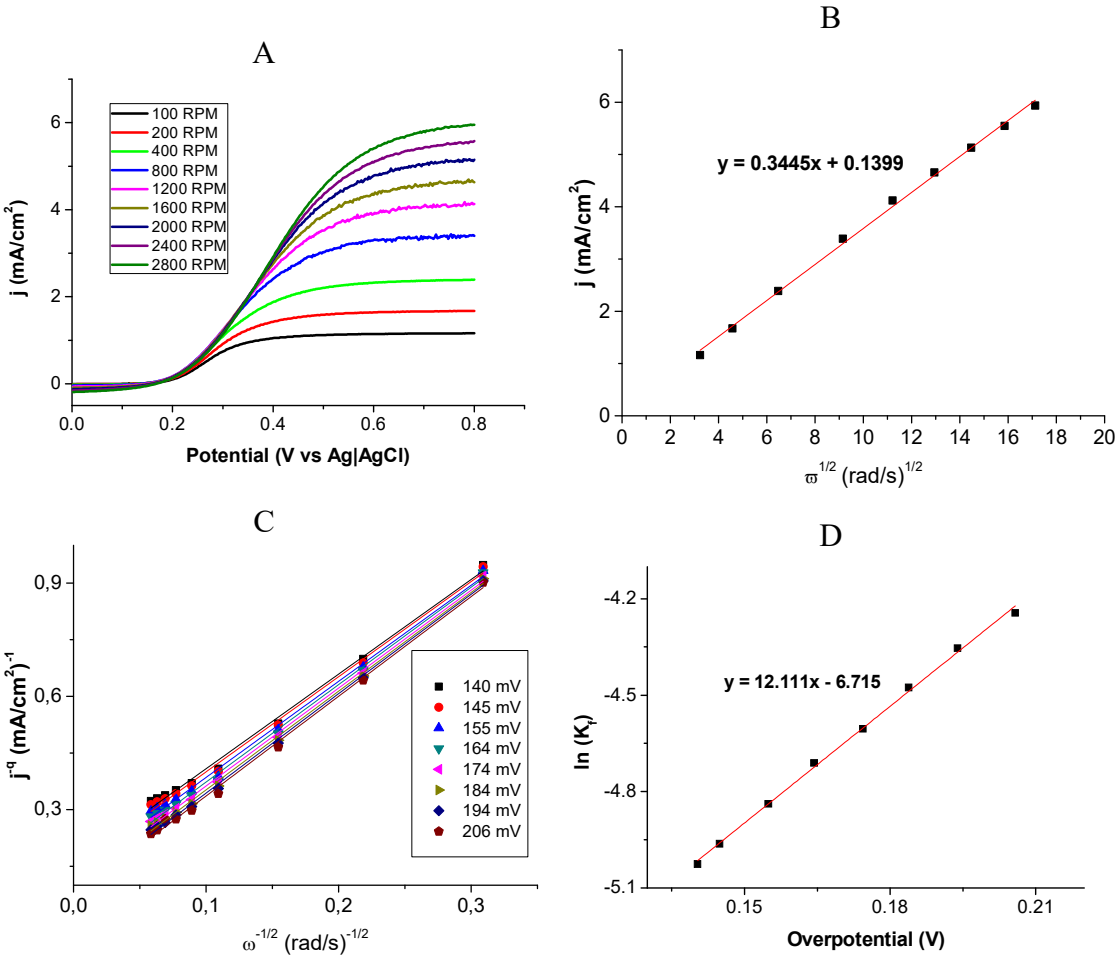

Figure S3: RDE analysis of **$Na_4[Fe(CN)_6]$** 10mM in 1M NaCl electrolyte on glassy carbon working electrode: (a) LSV scans with rotating disc working electrode; Scan rate: 5 mV/s (b) Levich analysis of the oxidation limiting currents; (c) Koutecký-Levich plot (b) and Tafel-plot for different overpotentials

1.4 Membrane permeability tests

The permeability of cation exchange membrane for AQDS and $Na_4[Fe(CN)_6]$ was determined using a diffusion H-cell. A piece of pretreated and non-pretreated membrane (details described in section 1.5) of an effective area (4 cm^2) was sandwiched between two diffusion half-cells with the same volume. The left compartment – retentate - was filled with 100 mM of the corresponding RAM in 1 M NaCl (18 mL) and the right one – permeate - was only filled with 1 M NaCl solution (18 mL). The two solutions were continuously stirred to avoid the gradient concentration profile on the membrane surface. The composition of permeate was periodically evaluated was checked by UV–Vis spectrophotometer. The permeability of the membrane was then evaluated according to the Fick's law:

$$ln\frac{C_B}{C_B - C_A} = \frac{PA}{V_B l} \cdot t \qquad \text{(S5)}$$

where C_B is the RAM concentration in the retentate and C_A in the permeate solution, P is the membrane permeability (cm^2/s). A is the active area (cm^2), V_B is the volume of each tank (cm^3) and l is the thickness of membrane(cm).

On Figure S4 we show the calibration curve of the UV-Vis spectrometry for both AQDS and Ferrocyanide solutions. The absorbance values at different wavelengths were measured in order to avoid errors.

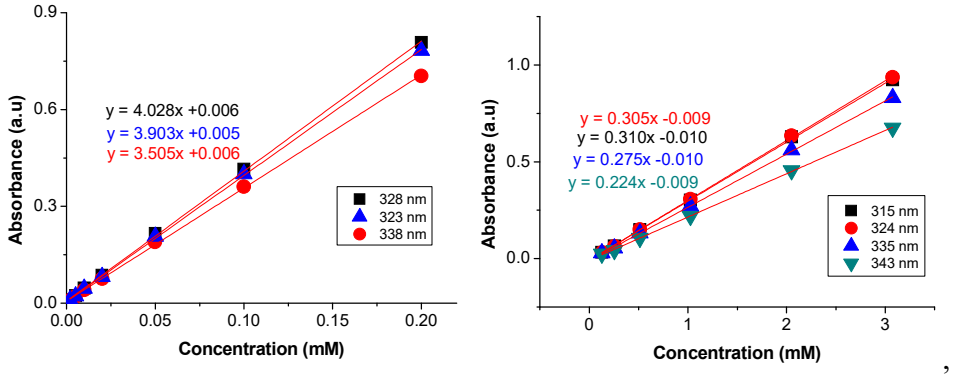

Figure S4: UV-Vis calibration curves at different wavelengths for the AQDS (left) and $Na_4[Fe(CN)_6]$ (right) .

1.5 Membrane pretreatment

The Nafion 212 membrane® was cut in pieces of the desired size. of 4x4cm to ensure the correct sealing in the cell. These pieces have been boiled for 1h in the following solutions: i) H_2O, ii) H_2O_2 3%, iii) H_2O, iv) H_2SO_4 water solution 0.5 M, v) H_2O. Between steps the membranes have been rinsed with water to remove the excess of the solution.

1.6 RFB single-cell testing

The flow cell was set up using two copper current collector plates, two composite bipolar plates (carbon-polyolefin), graphite felts electrodes (SGL GFD 4.6 EA, used as received), four sheets of gasket (flat, polyolefin) and Nafion 212® membrane from Dupont®. Membranes were soaked in 1 M of NaCl solution for 24 h prior to be used. The active area of the cell was 4 cm^2. A Watson-Marlow 323 peristaltic pump was used to circulate the electrolyte through the system at a flow rate of 40 mL/min. The reservoirs were purged

with Argon (99.999% purity) for 30 minutes to remove the O_2 before cycling. The whole system was placed inside a home-made glovebox which was purged with argon for 30 minutes. The cell was galvanostatically charged/discharged at room temperature using a Biologic multichannel potentiostatic-galvanostatic coupled to an impedance module BSC-815 in the voltage range of 0 - 1.1 V at various current densities (20, 40, 60, 80 and 100 mA/cm^2, 5 cycles) and cycled for 100 cycles at 80 mA/cm^2. This method was applied to ensure that both experiments have reached similar state of charge making the results comparable.

2. Performance and stability parameters

The understanding of the different RFB parameters as well as the experimental protocols is mandatory for further progress in the development of this technology. One of the most important things in this field is to understand the different parameters that show the quality of the battery performance. [1-3]

The Coulombic Efficiency (CE) describes the relationship between the total charge extracted from the battery during the discharging process and the charge supplied during the charge process (Eq. S6). All batteries have CE losses due to parasitic electrochemical and chemical reactions (hydrogen evolution, self-discharge reaction with oxygen), active species crossover and degradation of the active materials among others.

$$Coulombic\ Efficiency\ (CE) = \frac{Q_{discharge}}{Q_{charg}} = \frac{\int_0^t I_{discharge}\,dt}{\int_0^t I_{charg}\,dt} \quad \text{(S6)}$$

Voltage Efficiency (VE) is another important parameter to evaluate the battery efficiency. VE represents the ratio between the average discharge voltage to the average charge voltage and it is related to the operation current density, ionic conductivity of the membrane and electrolytes, electronic conductivity and catalytic activity of electrode materials, flow rate of electrolyte and mass transport of active species to the electrode surface (Eq. S7).

$$Voltage\ Efficiency\ (VE) = \frac{\bar{V}_{discharge}}{\bar{V}_{charg}} = \frac{\int_0^t V_{discharge}\,dt}{\int_0^t V_{charge}\,dt} \quad \text{(S7)}$$

The difference between these mean values is caused by a variety of overpotentials which have been widely studied by polarization curves (for discharge represented in Figure S5). The main contributions to the losses in a redox flow battery are i) activation losses, ii) ohmic (iR) losses and iii) mass transport losses. The first one is associated with the activation polarization of the electrodes, the main contribution appears at low current densities, and it is related with the kinetics of the charge transfer reaction (the energy needed to overcome the activation energy associated with the redox process in the electrode-electrolyte interfaces). The second causes a voltage drop is associated to resistance of the flow of electrons through the electrically conductive components and to the flow of ions through the membrane and electrolytes and can be expressed by Ohm´s law. Thus, in this region, the cell voltage linearly decreases with current densities. Finally, the last contribution is related with the lack of active material in the electrode surface proximity due to conversion at high current density significant decreasing the cell voltage.

The individual contribution of the overall cell resistance can be differentiated by Electrochemical Impedance Spectroscopy (EIS). This alternate current (AC) technique consists of a perturbation of a magnitude (current or voltage, GEIS or PEIS respectively) over a range of frequencies. After the impedance collection, the data can be fitted to various circuit models to identify the individual contributions to the total impedance (charge transfer resistance, mass transport, electrode process, etc.) [4]. The intercept in the real axis at low frequencies from the Nyquist plot corresponds to the ohmic resistance of the cell (R_Ω). This parameter includes the contribution of ohmic resistances of the ion exchange membrane, the carbon felt electrode ant the contact resistance between the bipolar plates and the felt electrodes. In the middle frequency range, the charge transfer resistance is observed (its value is proportional to width of the semicircle), while at low frequency range diffusion and mass transport are dominant. Furthermore, variation in the EIS during the battery cycling could suggest changes in polarization resistance associated with electrode modification, degradation of materials and optimizing parameters. [5] From the discharging polarization curve (Figure S5b), the power density (mW/cm^2) of the system can be calculated by multiplying the current density(j) with the cell potential (U). This parameter gives us a quick idea about optimal range of current densities with respect to its performance. Typically, these curves are measured under various conditions such as SOC, temperature or flow rate to see the effect of these parameters on the battery performance. Also, it can be significantly affected by the flow dynamic of the system. [6, 7]

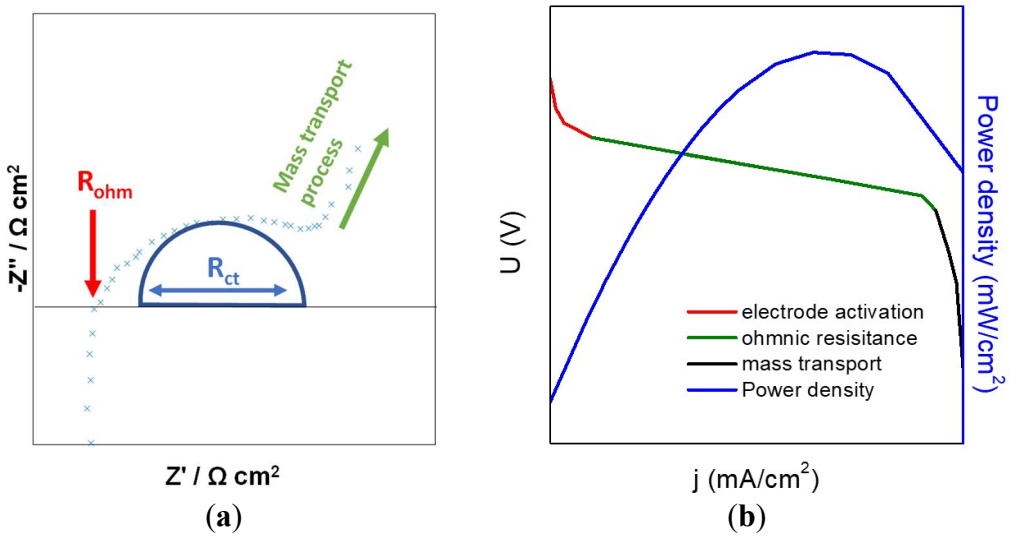

Figure S5. (a) Schematic representation of the different resistance identified in EIS of the whole system (b) Schematic representation of the discharging polarization curve showing the main losses regarding each resistance in the system and the power density achieved.

Finally, both parameters merge as a final parameter called Energy Efficiency (EE). EE is the relationship between energy stored during the charging and energy released during discharging processes (Eq. S8). Typical EE values of RFBs are in the range from 50 to 90%, depending on the applied current density, operating conditions, and internal component quality.

$$Energy\ Efficiency\ (EE) = CE \cdot VE = \frac{\int_0^t I_{discharge} \cdot \overline{V}_{discharge} \cdot dt}{\int_0^t I_{char} \cdot \overline{V}_{charg} \cdot dt} \quad \text{(S8)}$$

The redox flow battery can work at different operation mode, one of the mostly used methods to charge/discharge the battery is carried out galvanostatically, i.e., at constant current, until the battery reaches the given charging or discharging voltage limits (cut-offs). The use of higher currents to charge/discharge the battery leads to use smaller share of theoretical capacity of the active material (i.e., lower capacity utilization, Eq. S9), because higher currents involve higher overpotential in the system (and thus the charging voltage limit is reached at lower SOC, and similarly for discharging).

Capacity utilization is the relationship between the practical capacity storage in the system *vs*. the theoretical capacity that could be stored at a given testing condition and it is calculated by Eq.S9:

$$Capacity\ Utilization\ (CU) = \frac{Q_{discharge}}{Q_{theoretical}} \quad \text{(S9)}$$

Where the $Q_{theoretical}$ is equal to the moles of electrons that the redox active material in the limiting side can store (Faraday's law).

For most RFB technologies, U-j dependence is linear in a relatively broad range of current densities and thus so-called Area Specific Resistance (ASR) parameter can be used to describing the battery performance under given conditions (SOC, electrolyte flow rate, temperature etc.) (Eq. S10). It provides information about the total resistance of the cell, and its units are Ohm·cm^2. ASR represents the resistances of the different contacts, current collectors, bipolar plates, carbon felts, electrolyte, and membrane contributions. It can be determined following Ohm's Law and can be calculated from the linear part of the Load Curves (LC). It gives an idea about the resistance under current load during charging and discharging processes under given conditions (temperature, such as electrolyte flow velocity, SOC) and includes the contribution of the ohmic, charge transfer and mass transport polarization in the cell. Once the electrode activation process has been overcome, the resistance between the electrolyte and electrode decreases. ASR can be evaluated from the linear part of the load curves according to Eq. S10:

$$Area\ Specific\ Resistance\ (ASR) = \frac{V_2 - V_1}{I_2 - I_1} \cdot A \quad \text{(S10)}$$

3. Experimental aspects

Setting up a RFB is relatively easy, but some technical considerations must be done. The membrane should be conditioned in the desire supporting electrolyte in order to prevent further volume changes due to the membrane swelling and possible contamination of the electrolytes by counterions. For most of the RFB chemistries, carbon felt electrodes should be oxidatively treated, which is typically done by thermal treatment in oxygen atmosphere (to increase the hydrophilicity and potential catalytic activity) and cleaned with EtOH (to remove the dust and the impurities potentially decreasing the accessible surface for electrochemical reactions or catalysing parasitic reactions such as water splitting). Finally, before starting to pump the electrolytes into the system, all connections must be properly tightened, and the system needs to be purged by passing argon or

nitrogen gas for at least 30 minutes through the solutions and the cell in order to remove all the oxygen present in the system.

So far, no standardized procedure has been proposed for RFB testing among the variety of established works protocols for the study of RFBs. Herein, we propose a relatively complex and universal procedure that can be used to check the performance of new RFB systems to provide representative information about battery performance and mid-term stability. The procedure followed is:

1) Deareation of the electrolytes and apparatus by nitrogen
2) Evaluation of the initial pH of the catholyte and anolyte
3) Characterization of the cell by EIS at 0% SOC
4) Galvanostatic cycling measurements: 5 cycles charging/discharging at each constant current density of 20, 40, 60, 80 and 100 mA/cm^2.
5) Mid-term stability study: 100 galvanostatic cycles at the higher current density (100 mA/cm^2) to evaluate the capacity decay over time and per cycle.
6) Characterization of the cell by EIS at 0% SOC after cycling.
7) Evaluation of the pH and volume on each tank after the cycling
8) Determination of the cross-over of RAM on each tank.

The comparison between EIS measurements before and after cycling could help us to understand the change in the membrane and felts conductivity. A critical change in the ionic conductivity may indicate on a membrane (micro)fracture or fouling and/or deposition of the electrolyte in the felt blocking its the active area.

The battery performance at different current densities provides useful information about the individual efficiencies (CE, VE, EE) of the initial cell, while trend in capacity utilization, within mid-term cycling at selected current density is mainly done to assess the capacity decay, i.e. battery stability under given cycling conditions. Usually, charging the battery at low current densities lead to higher capacity utilization (as charging voltage cut-off is reached at higher SOC) but also higher capacity decay due to typically lower stability of charged form of RAM. Thus, higher concentration of charged species which are more reactive lead typically to faster degradation of redox active materials. [8] On the other side, charging at higher current densities leads to lower voltage and energy efficiencies and capacity utilization due to higher *iR* drops. Finally, long-term stability could be studied by performing 100 charge/discharge cycles at constant current density and checking how the capacity evolves. The capacity decay could be related to the decomposition/deposition and crossover of RAM or SOC disbalance due to parasitic reactions (water splitting, self-discharge by oxygen). For galvanostatic cycling, capacity can be also significantly affected by variation of cell resistance (affecting SOC range reached in the individual cycle). This can be prevented by application of combined galvanostatic cycling with potentiostatic hold at given voltage cut-offs until current density drops below limit value (e.g., 10% of the value used for galvanostatic period).

The EIS measurements can be combined also with polarization (load) curve measurements at various SOC (50% SOC is typically used) to provide more complex information regarding the distribution of the efficiency losses within the cell.

4. Single-cell testing – supplementary results

In the following section the experimental data from single-cell battery testing are summarized in addition to the data presented within the main manuscript

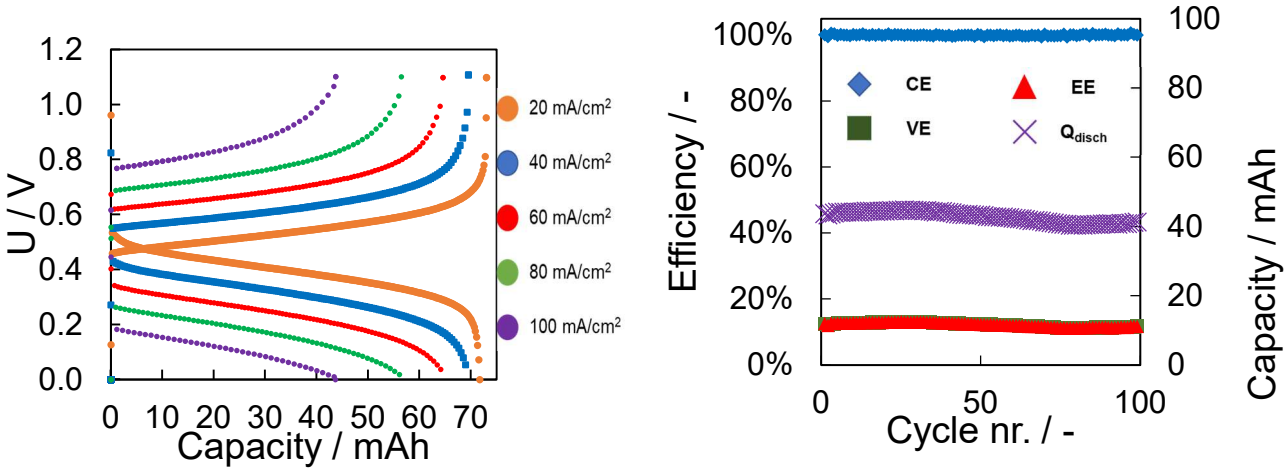

(**a**) (**b**)

Figure S6: (a) E_{cell} vs Capacity plot at different current densities (20, 40, 60, 80 and 100 mA/cm^2) for the battery using 0.08M AQDS in **1 M acetate buffer (pH 4.5)** (2.45 g sodium acetate + 7mL of acetic acid to 100 mL) *vs* 0.2 M $Na_4[Fe(CN)_6]$ in **1 M acetate buffer (pH 4.5)** as electrolytes and N212® pretreated membrane inside homemade glovebox. (b) Coulombic, Voltage, Energy Efficiencies and $Q_{discahrge}$ for the battery cycle 100 cycles at 100 mA/cm^2 using 0.08 M AQDS in acetate buffer 1 M (pH 4.5) *vs* 0.2 M $Na_4[Fe(CN)_6]$ in **acetate buffer 1 M (pH 4.5)** as electrolytes and N212® pretreated membrane inside homemade glovebox.

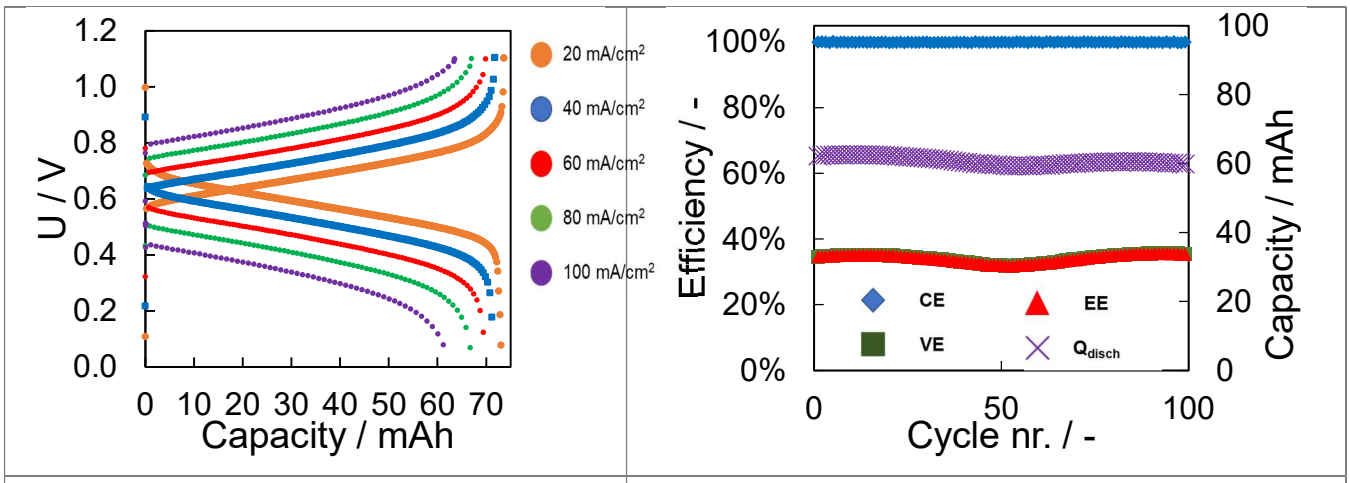

(**a**) (**b**)

Figure S7: (a) E_{cell} vs Capacity plot at different current densities (20, 40, 60, 80 and 100 mA/cm^2) for the battery using 0.08 M AQDS in 1 M **phosphate buffer 1 M (pH 7.5)** *vs* 0.2 M $Na_4[Fe(CN)_6]$ in **phosphate buffer 1 M (pH 7.5)** (9.01 g NaH_2PO_4 and 6.00 g Na_2HPO_4 to 100mL) as electrolytes and N212® pretreated membrane inside homemade glovebox. (b) Coulombic, Voltage, Energy Efficiencies and $Q_{discahrge}$ for the battery cycle 100 cycles at 100 mA/cm^2 using 0.08 M AQDS in **phosphate buffer 1 M (pH 7.5)** *vs* 0.2 M $Na_4[Fe(CN)_6]$ in **phosphate buffer 1 M (pH 7.5)** as electrolytes and N212® pretreated membrane inside homemade glovebox.

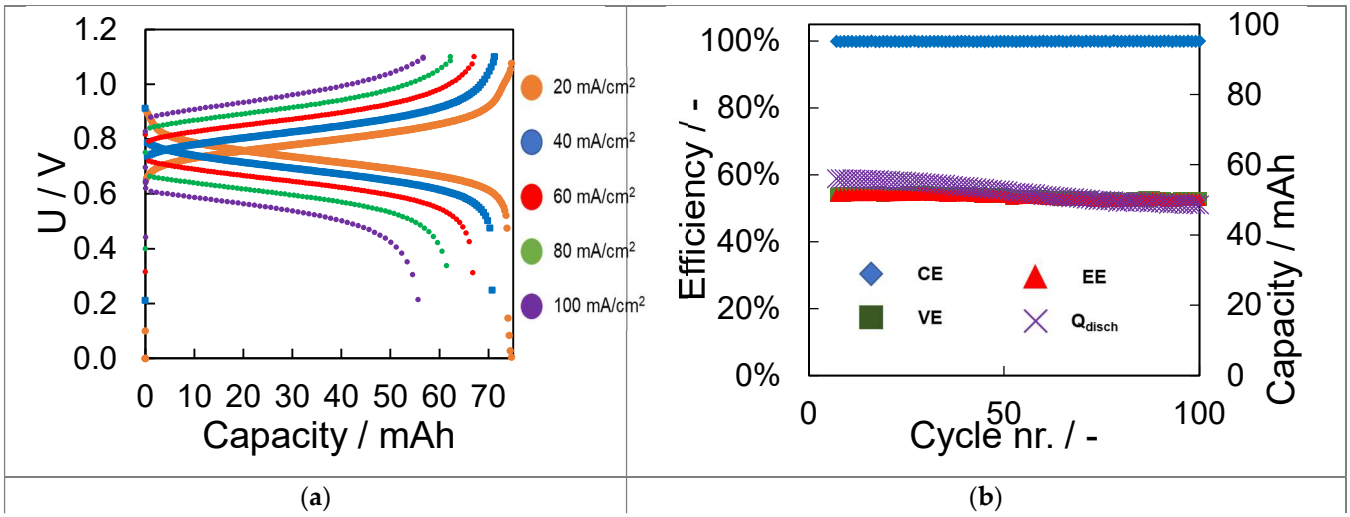

(**a**) (**b**)

Figure S8: (a) E_{cell} vs Capacity plot at different current densities (20, 40, 60, 80 and 100 mA/cm^2) for the battery using 0.08 M AQDS in 1 M **carbonate buffer 1 M (pH 10.5)** *vs* 0.2 M $Na_4[Fe(CN)_6]$ in **carbonate buffer 1 M (pH 10.5)** (3.88 g NaHCO3 and 5.71 g to 100 mL) as electrolytes and N212® pretreated membrane inside homemade glovebox. (b) Coulombic, Voltage, Energy Efficiencies and $Q_{discahrge}$ for the battery cycle 100 cycles at 100 mA/cm^2 using 0.08 M AQDS in **carbonate buffer 1 M (pH 10.5)** *vs* 0.2 M $Na_4[Fe(CN)_6]$ in **carbonate buffer 1 M (pH 10.5)** as electrolytes and N212® pretreated membrane inside homemade glovebox.

Table S1: Coulombic, voltage, energy efficiencies and capacity decay at different current densities for the battery at different pH.

pH	*I* (mA/cm^2)	CE (%)	VE (%)	EE (%)	CU (%)	Capacity decay (mAh/cycle)	Capacity decay (%$Q_{theor.}$/cycle)
pH 4	20	96.8	70.0	67.8	89.4	-0.962	-1.12
	40	99.8	47.1	47.0	81.2	-0.06	-0.07
	60	100	32.1	32.1	75.2	0.036	0.04
	80	100	21.2	21.2	65.6	0.022	0.03
	100 (100c)	100	12.2	12.2	53.3	-0.049	-0.06
pH 7	20	99.4	81.8	81.3	87.3	-0.192	-0.22
	40	99.8	66.3	66.2	83.7	-0.045	-0.05
	60	100	54.1	54.1	81.2	0.01	0.01
	80	100	44.0	44.0	77.9	0.045	0.05
	100 (100c)	100	34.1	34.1	74.5	-0.028	-0.03
pH 10	20	98.9	88.0	87.0	89.5	0.142	0.17
	40	99.7	79.0	78.7	83.5	-0.153	-0.18
	60	99.8	69.9	69.8	78.5	-0.157	-0.18
	80	99.9	61.4	61.4	72.5	-0.071	-0.08
	100 (100c)	99.9	53.4	53.4	66.7	-0.092	-0.11

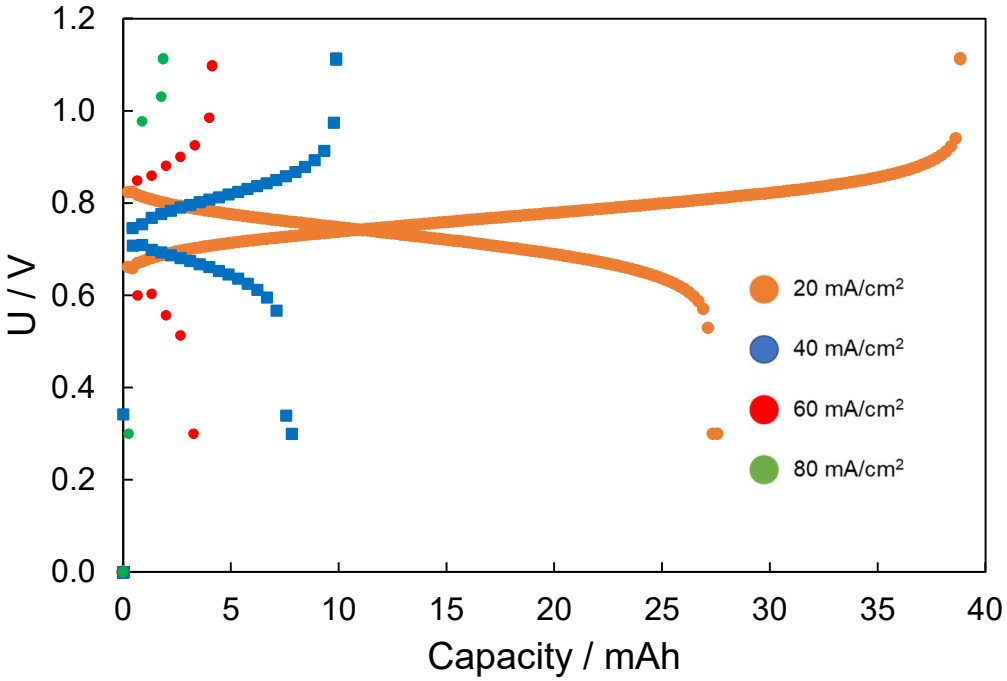

Figure S9: (a) E_{cell} vs Capacity plot at different current densities (20, 40, 60, 80 mA/cm^2) for the battery using 0.1 M AQDS in 1 M NaCl *vs* 0.1 M $Na_4[Fe(CN)_6]$ in 1 M NaCl as electrolytes and N212® pretreated membrane, **measured exposed to atmospheric concentrations of O_2**.

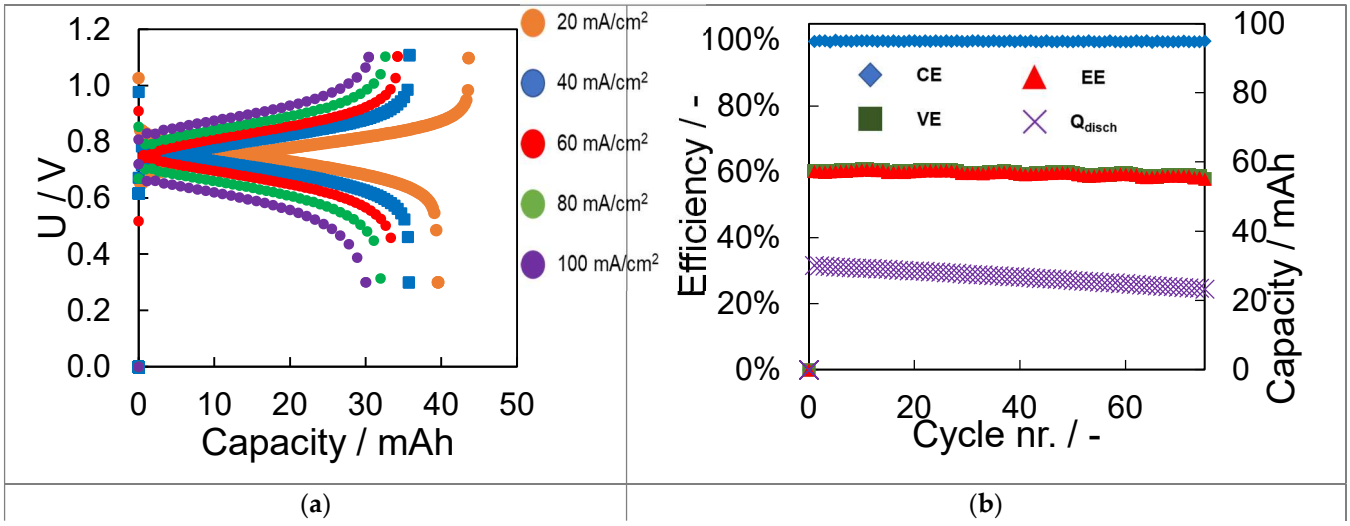

(**a**) (**b**)

Figure S10: (a) E_{cell} vs Capacity plot at different current densities (20, 40, 60, 80 and 100 mA/cm^2) for the battery using. (b) Coulombic, Voltage, Energy Efficiencies and $Q_{discahrge}$ for the battery cycle 100 cycles at 100 mA/cm^2 using 0.1 M AQDS in 1 M NaCl *vs* 0.1 M $Na_4[Fe(CN)_6]$ in 1 M NaCl as electrolytes and N212® pretreated membrane **measured inside homemade glovebox**.

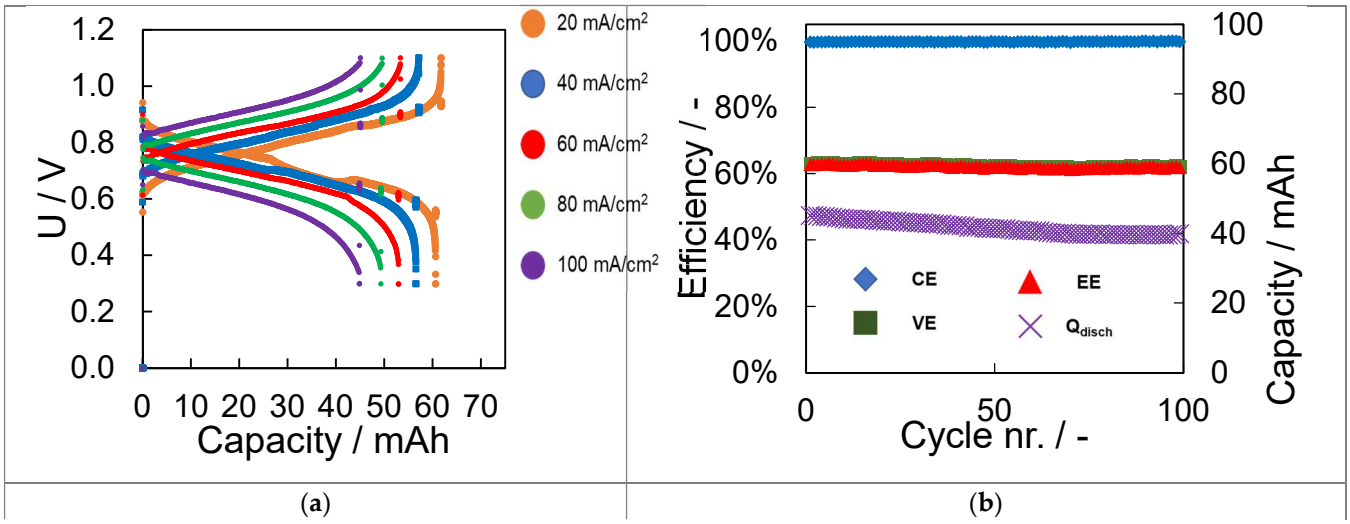

(**a**) (**b**)

Figure S11: (a) E_{cell} vs Capacity plot during galvanostatic cycling at different current densities (20, 40, 60, 80 and 100 mA/cm^2) and (b) Coulombic, Voltage, Energy Efficiencies and $Q_{discahrge}$ evaluated from galvanostatic cycling at 100 mA/cm^2 for a battery using 0.1 M AQDS in 1 M NaCl *vs* 0.1 M $Na_4[Fe(CN)_6]$ in 1 M NaCl as electrolytes and N212® pretreated membrane, **measured inside commercial nitrogen-filled glovebox**.

Table S2: Coulombic, voltage, energy efficiencies and capacity decay at different current densities for the battery exposed to different concentrations of O_2.

O_2	*I* (mA/cm^2)	CE (%)	VE (%)	EE (%)	CU (%)	Capacity decay (mAh/cycle)	Capacity decay (%$Q_{theor.}$/cycle)
Exposed to atmospheric O_2 concetrations	20	79.3	84.0	66.6	41.1	-4.01	-6.00
	40	90.2	65.8	59.3	10.5	-0.51	-0.76
	60	92.0	48.3	44.4	4.5	-0.234	-0.35
	80	62.3	1.14	0.77	2.3	-1.3	1.87
	100 (100c)	---	---	---	---	---	---
Home-made glovebox	20	97.8	90.0	88.1	59.1	-0.81	-1.2
	40	99.7	83.1	82.8	53.1	-0.17	-0.26
	60	99.7	75.2	75.0	50.4	-0.13	-0.29
	80	99.7	67.6	67.5	48.1	-0.12	-0.18
	100 (100c)	99.8	60.3	60.1	44.9	-0.09	-0.14
Commercial glovebox	20	99.5	69.5	69,1	93.2	-0.º	-0.44
	40	99.0	82.8	82.0	85.7	-0.392	-0.58
	60	99.3	76.7	76.1	80.2	-0.29	-0.43
	80	99.5	69.5	69.1	74.2	-0.071	-0.08
	100 (100c)	99.6	63.1	63.9	67.4	-0.062	-0.09

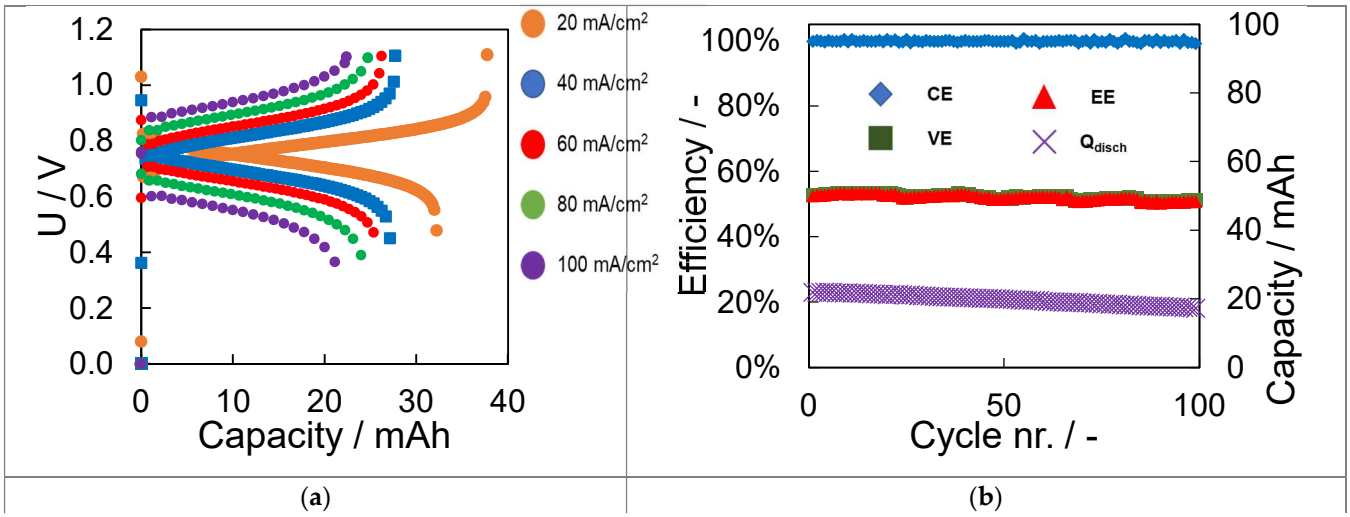

(**a**) (**b**)

Figure S12: (a) E_{cell} vs Capacity plot at different current densities (20, 40, 60, 80 and 100 mA/cm^2) and (b) Coulombic, Voltage, Energy Efficiencies and $Q_{discahrge}$ for the battery cycle 100 cycles at 100 mA/cm^2 using 0.1 M AQDS in 1 M NaCl *vs* 0.1 M $Na_4[Fe(CN)_6]$ in 1 M NaCl as electrolytes and N212® **non-pretreated membrane** inside home-made glovebox.

Table S3: Coulombic, voltage, energy efficiencies and capacity decay at different current densities for the battery using the pretreated or non-pretreated membrane.

O_2	*I* (mA/cm^2)	CE (%)	VE (%)	EE (%)	CU (%)	Capacity decay (mAh/cycle)	Capacity decay (%$Q_{theor.}$/cycle)
Pretreated	20	97.8	90.0	88.1	59.1	-0.81	-1.2
	40	99.7	83.1	82.8	53.1	-0.17	-0.26
	60	99.7	75.2	75.0	50.4	-0.13	-0.29
	80	99.7	67.6	67.5	48.1	-0.12	-0.18
	100 (100c)	99.8	60.3	60.1	44.9	-0.09	-0.14
NON-pretreated	20	97.8	89.0	87.0	48.4	-1.09	-1.63
	40	99.8	79.0	78.9	40.6	-0.1	-0.15
	60	99.9	69.6	69.5	38.6	-0.05	-0.07
	80	99.8	61.3	61.2	36.4	-0.05	-0.07
	100 (100c)	99.8	52.9	52.8	32.7	-0.05	-0.07

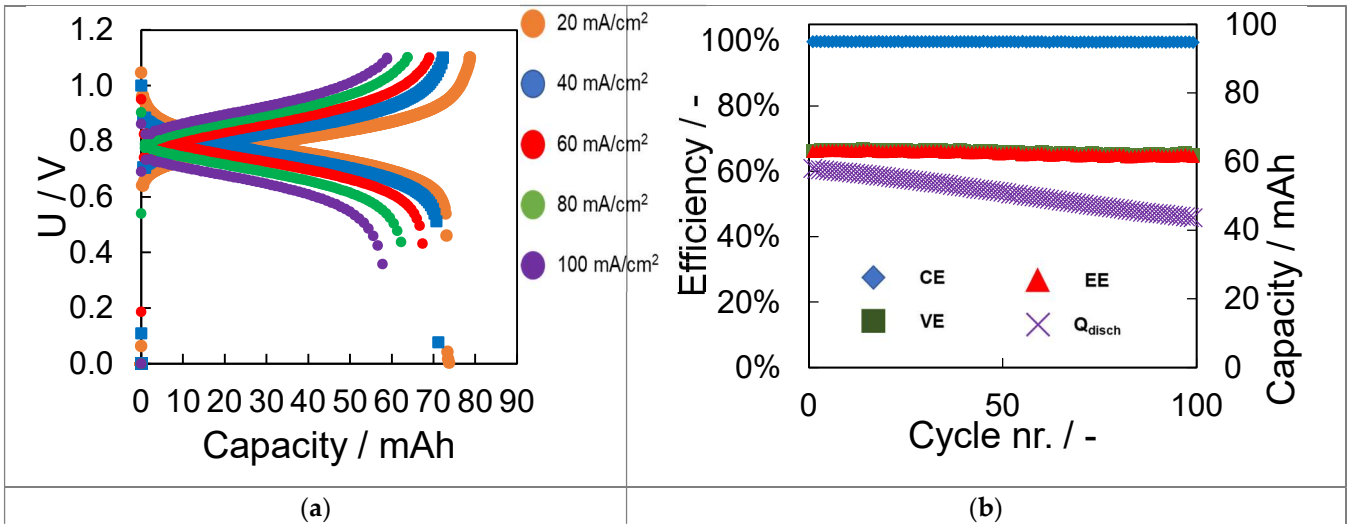

(a) (b)

Figure S13: (a) E_{cell} vs Capacity plot at different current densities (20, 40, 60, 80 and 100 mA/cm^2) for the battery using 0.08M AQDS in 1 M NaCl *vs* 0.2 M $Na_4[Fe(CN)_6]$ in 1 M NaCl as electrolytes. (b) Coulombic, Voltage, Energy Efficiencies and $Q_{discahrge}$ for the battery cycle 100 cycles at 100 mA/cm^2 using 0.08 M AQDS in 1 M NaCl *vs* 0.2 M $Na_4[Fe(CN)_6]$ in 1 M NaCl as electrolytes and N212® pretreated membrane inside homemade glovebox.

Table S4: Coulombic, voltage, energy efficiencies and capacity decay at different current densities for the battery being the catholyte and the anolyte the capacity limiting side.

CLS	*I* (mA/cm^2)	CE (%)	VE (%)	EE (%)	CU (%)	Capacity decay (mAh/cycle)	Capacity decay (%$Q_{theor.}$/cycle)
Anolyte	20	97.8	90.0	88.1	59.1	-0.81	-1.2
	40	99.7	83.1	82.8	53.1	-0.17	-0.26
	60	99.7	75.2	75.0	50.4	-0.13	-0.29
	80	99.7	67.6	67.5	48.1	-0.12	-0.18
	100 (100c)	99.8	60.3	60.1	44.9	-0.09	-0.14
Catholyte	20	98.0	91.5	89.7	89.0	0.283	0.33
	40	99.0	85.1	84.3	83.4	-0.21	-0.24
	60	99.3	78.9	78.4	78.7	-0.28	-0.32
	80	99.6	72.7	72.4	73.3	-0.164	-0.19
	100 (100c)	99.7	66.6	66.4	67.5	-0.151	-0.18

5. References

[1] Ghimire, P. C.; Bhattari, A.; Lim, T. M.; Wai, N.; Skyllas-Kazacos, M.; Yan, Q. In-Situ Tools Used in Vanadium Redox Flow Battery. *Batteries* **2021**, *7*, 53-89.

[2] Yao, Y.; Lei, J.; Ai, F.; Lu, Y.-C. Assessment methods and performance metrics for redox flow batteries. *Nature Energy* **2021**, *6*, 582-588.

[3] Li, M.; Odom, S. A.; Pancoast, A. R.; Robertson, L. A.; Vaid, T. P.; Agarwal, G.; Doan, H. A.; Wang, Y.; Suduwella, T. M.; Bheemireddy, S. R.; Ewoldt, R. H.; Assary, R. S.; Zhang, Lu,

Sigman, M. S.; Minteer, S. D. Experimental Protocols for Studying Organic Non-aqueous Redox Flow Batteries. ACS Energy Lett. **2021**, *6*, 3932–3943.

[4] Baricci, A.; Zago, M.; Casalegno, A. Modelling analysis of heterogenity og ageing in high temperature polymer electrolyte fuel cells. Insights into of electrochemical impedance spectra. *Electrochim. Acta* **2016**, *222,*596-607.

[5] Wagner, N.; Gülzow, E. Change of electrochemical impedance spectra (EIS) with time during CO-poisoning of the Pt-anode in membrane fuel cell. *J. Power Sources* **2004**, *127*, 341-347.

[6] Ke, X.; Prahl, J. M.; D. Alexander, J. I.; Wainright, J. S.; Zawodzinski, T. A.; Savinell, R. F. Rechargeable redox flow batteries: flow fields, stacks and design considerations. *Chem. Soc. Rev.* **2018**, *47,* 8721-8743.

[7] Zheng, Q.; Xing, F.; Li, X.; Ning, G.; Zhang, H. Flow feld design and optimization based on the mass transport polarization regulation in a fow-through type vanadium fow battery. *J. Power Sources* **2016**, *324*, 402-411.

[8] Kwabi, D. G.; Ji, Y.; Aziz, M. J. Electrolyte Lifetime in Aqueous Organic Redox Flow Batteries: A Critical Review. *Chem. Rev.* **2020**, *120*, 6467-6489.